Combined toxicity of graphite-diamond nanoparticles and thiabendazole to *Daphnia magna*

Please, cite as follows:

Idoia Martín-de-Lucía, Sandra F. Gonçalves, Francisco Leganés, Francisca Fernández-Piñas, Roberto Rosal, Susana Loureiro, Combined toxicity of graphite-diamond nanoparticles and thiabendazole to *Daphnia magna*, Science of The Total Environment, Volume 688, 2019, Pages 1145-1154, https://doi.org/10.1016/j.scitotenv.2019.06.316.

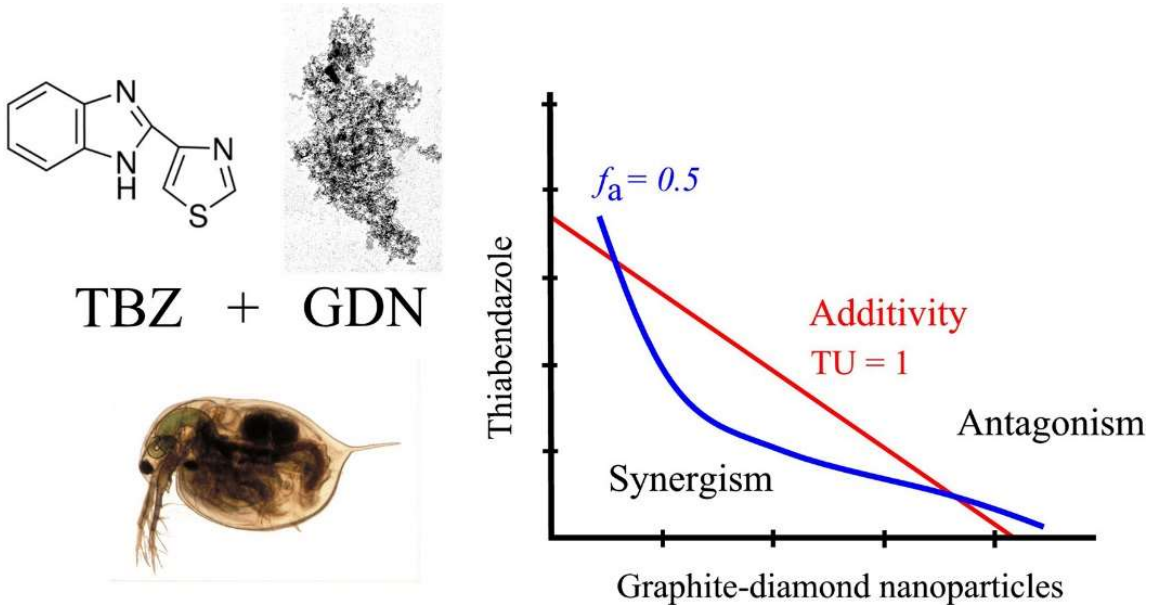

Link to official URL: http://www.sciencedirect.com/science/article/pii/S004896971932889X

Combined toxicity of graphite-diamond nanoparticles and thiabendazole to *Daphnia magna*

Idoia Martín-de-Lucía[1], Sandra F. Gonçalves[2], Francisco Leganés[3], Francisca Fernández-Piñas[3], RobertoRosal[1,*], SusanaLoureiro[2,*]

[1] Department of Chemical Engineering, University of Alcalá, E-28871 Alcalá de Henares, Madrid, Spain
[2] Department of Biology & CESAM, University of Aveiro, Campus Universitario de Santiago, 3810-193 Aveiro, Portugal
[3] Department of Biology, Universidad Autónoma de Madrid, E-28049 Madrid, Spain

[*] Corresponding authors: roberto.rosal@uah.es, sloureiro@ua.pt

Abstract

Carbon-based nanomaterials exhibit unique properties that make them suitable for a wide variety of industrial and biomedical applications. In this work, we studied the acute toxicity of graphite-diamond nanoparticles (GDN) combined with the fungicide thiabendazole (TBZ) to the immobilization of the cladoceran *Daphnia magna* in the presence and absence of the micro green algae *Raphidocelis subcapitata*, supplied as food source. The toxicity of GDN to *D. magna* decreased in the presence of *R. subcapitata*, while that of TBZ increased, the latter suggesting a carrier effect to TBZ. GDN-TBZ mixtures were fitted to the most common conceptual models applied to mixture toxicity: Concentration Addition (CA), Independent Action (IA) and Combination Index (CI). For GDN-TBZ mixtures in the absence of food the best fit was obtained with dose ratio deviation from CA model, while in the presence of food, dose level deviation from CA gave a better fit. The binary mixtures of GDN and TBZ showed synergistic toxic interactions at low concentrations, which could be attributed to the increased bioavailability of TBZ adsorbed on GDN. For higher concentrations of GDN, the binary mixtures turned antagonistic due to particle agglomeration. Our study provides evidence that deviations from additivity are dose dependent and relevant for the risk assessment of mixtures of nanoparticles with other chemical pollutants.

Introduction

With the recent developments in nanotechnology, carbon-based nanomaterials such as fullerenes, carbon nanotubes (CNT), graphene, nanodiamonds and graphite nanoparticles, are becoming key materials for many industrial and biomedical uses (De Volder et al., 2013; Mundra et al., 2014). Nanodiamonds exhibit the well-known features of nanomaterials, which include high surface area, tunable surface chemistry, excellent biocompatibility and superior mechanical and optical properties. Considered altogether, these properties make nanodiamonds suitable for a wide range of applications (Kumar et al., 2019; Mochalin et al., 2011; Schrand et al., 2009). In fact, nanodiamonds are one of the few nanomaterials produced at real industrial scale, although their synthesis is difficult due to the extreme conditions required and because the diamond phase is inherently unstable (Nian et al., 2014). Industrial nanodiamonds are not pure. Instead, they consist of an ordered diamond (sp^3) core sheltered by a stabilizing graphitic (sp^2) layer with different proportions of impurities and oxygen-containing surface functional groups (Bradac and Osswald, 2018).

Despite its growing market possibilities, the toxicity of nanodiamonds has received limited attention so far (van der Laan et al., 2018). Nanodiamonds were found non-toxic for tumour cell lines, while graphite nanoparticles exhibited cytotoxicity (Zakrzewska et al., 2015). Wierzbicki et al. demonstrated that both diamond and graphite nanoparticles inhibit the formation of new blood vessels, called angiogenesis, a crucial process involved in cancer progression (Wierzbicki et al., 2013). As for their environmental impact, it has been pointed out that invertebrates can be particularly sensitive to nanodiamonds, which makes them appropriate to study the potential hazard of nanodiamonds (Karpeta-Kaczmarek et al., 2018). Mendonça et al. studied the toxicity of diamond nanoparticles to the survival and reproduction of the cladoceran *Daphnia magna*. Their results showed reproduction inhibition at concentrations above 1.3 mg/L. The damage was attributed to the adhesion of the nanoparticles to the exoskeleton and to the gastrointestinal tract, the latter possibly blocking food absorption (Mendonça et al., 2011).

Nanomaterials are not the only emerging pollutants entering aquatic ecosystems. Once released, they may interact with other substances, including many anthropogenic chemicals. Thiabendazole (TBZ, 2-(4-thiazolyl)-1H-benzimidazole) is a benzimidazole derivative initially used as veterinary anthelmintic (Brown et al., 1961). It is also a broad-spectrum fungicide, used for controlling fungal fruit and

vegetable diseases (Robinson et al., 1969). Because of its extensive use in agricultural areas, TBZ can be released and widely dispersed and end up in aquatic ecosystems. TBZ was detected in 25% of the surface water samples taken from different rivers of the Ebro River basin with concentrations reaching 49 ng/L (Ccanccapa et al., 2016). As it happens with many other pollutants, TBZ is not completely removed in wastewater treatment plants. Consequently, TBZ has been frequently detected in their effluents, which constitute an important way of entry to the aquatic environment (Tran et al., 2018). The Environmental Protection Agency (EPA) has classified TBZ as highly toxic to freshwater fish and invertebrates (EPA, 2002).

The cladoceran *D. magna*, is a freshwater crustacean widely used as model organism in ecotoxicity tests. Aquatic filter feeders constitute a key group at the base of the food chains as primary consumers within freshwater ecosystems. Daphnids co-occur with algae in the aquatic environment, which constitute the main food source for zooplankton. It has been recognized that food limitation increases the sensitivity of freshwater zooplankton to contaminants (Antunes et al., 2003; Pieters and Liess, 2006). It is also well-known that food levels and their availability vary significantly under different environmental conditions (Pereira and Gonçalves, 2007). Algae can increase or decrease the toxicity of different compounds by changing their bioavailable for daphnids (Taylor et al., 1998). Therefore, testing different feeding conditions in filter feeder organisms is relevant since the different conditions may induce changes in the toxic responses of the organisms to contaminants (Hansen et al., 2008). In addition, it has been reported that the toxicity of silver nanoparticles to *D. magna* significantly decreases in the presence of food (Ribeiro et al., 2014).

Aquatic organisms in natural environments are commonly exposed to complex combinations of many contaminants, including nanomaterials (Jośko et al., 2017; Lopes et al., 2016). It has been shown that the co-occurrence of nanoparticles and micropollutants may result in non-additive interaction effects, even if the individual compounds are present at low concentrations (Martín-de-Lucía et al., 2018). The reference concepts, Concentration-Addition (CA) and Independent-Action (IA), are widely applied to estimate joint mixture toxicity (Jonker et al., 2005; Loureiro et al., 2010; Silva et al., 2018). CA model assumes that the individual components share a similar mode of action, while IA applies to mixtures of components with dissimilar modes of action. Recently, the Combination Index (CI)-isobologram method has been proposed to quantify deviations from additivity using a theoretical background taken from pharmacology (Martín-de-Lucía et al., 2018; Martín-de-Lucía et al., 2017; Rosal et al., 2010). The co-occurrence of anthropogenic pollutants with incipient regulatory status in water and wastewater poses an important threat as mixture toxicity is difficult to integrate into regulatory frameworks (Godoy and Kummrow, 2017). The mainstream opinion is that the toxicological interactions of wastewater pollutants are generally negligible and, therefore, CA predicts mixture toxicity with sufficient accuracy for regulatory purposes (EU, 2012). However, it has been shown that non-additive interactions do occur in mixtures of chemicals and nanoparticle at least because of pollutants adsorption onto the nanoparticle surface (Martín-de-Lucía et al., 2018; Sanchís et al., 2016). The purpose of this work was to provide additional data to fill in the knowledge gap on this topic by assessing the combined acute toxicity of graphite-diamond nanoparticles (GDN) and TBZ towards the freshwater crustacean *D. magna*. The experiments were conducted in the presence and absence of the microgreen algae *Raphidocelis subcapitata*, to evaluate the influence of different feeding conditions. The combined toxicity of GDN-TBZ was analysed using the CA, IA and CI-isobologram models to elucidate the deviations from additivity for the different concentrations, toxicant ratios and affected fractions.

2. Materials and methods

2.1. Test chemicals and analytical methods

Graphite-diamond nanoparticles (GDN, 20% minimum diamond content, ash content <0.3%, 4 nm average particle size) were supplied from PlasmaChem (Germany) free of metals and organic impurities. Stocks of GDN (500 mg/L) were prepared in Milli-Q water using ultrasonic dispersion for 1 h followed by 48 h stirring at room temperature. For it we used an ultrasonic bath with sine-wave modulation that delivered ultrasonic peaks of 600 W. Test GDN suspensions were prepared immediately before being used in characterization and toxicity assays by dispersing stocks as appropriate. The characterization of GDN suspensions (10 mg/L) was performed in ultrapure water (Milli-Q), OECD algal culture medium, and ASTM hard water medium. Hydrodynamic particle size and ζ-potential were measured using dynamic light scattering (DLS) and electrophoretic light scattering in a Zetasizer Nano apparatus (Malvern Instruments) at 25 °C. During characterization, GDN suspensions were kept at the same conditions (temperature, illumination, and agitation) used in toxicity experiments and a minimum of 9 replicates were performed.

Thiabendazole (TBZ, CAS number 148-79-8) ≥99 % purity was purchased from Sigma-Aldrich. Fresh stocks (50 mg/L) were prepared in ultrapure water with 0.1% v/v dimethyl sulfoxide (DMSO) a few minutes before each toxicity assay. The stock solutions were

subsequently diluted in OECD algal culture medium and ASTM hard water medium to obtain the appropriate concentrations for the *R. subcapitata* and *D. magna* toxicity bioassays.

Transmission electronic micrographs (TEM) were taken in a JEOL JEM-1400 1400 apparatus. Optical micrographs were recorded using an Eclipse E200-LED Nikon microscope. Attenuated Total Reflectance Fourier Transform Infrared (ATR-FTIR) spectra were obtained in a Thermo Scientific Nicolet iS10 apparatus with a Smart iTR-Diamond ATR module.

2.2. Biotests and culture conditions

The freshwater crustacean *D. magna*, clone K6, was taken from the cultures maintained at the University of Aveiro, Portugal. *D. magna* cultures were maintained in 1 L glass beakers (20 individuals/beaker) with 800 mL of ASTM (American Society for Testing and Materials) hard water medium (ASTM, 2014). The culture medium was renewed and daphnids were fed three times per week with *R. subcapitata* (3×10^5cells/mL) and a seaweed extract (6 mL/L added as supply of micronutrients). Cultures were kept in controlled laboratory conditions, at a temperature of 20 ± 1 °C and photoperiod cycle of 16-hour light:8-hour dark. Acute toxicity was assessed according to the OECD 202 guideline (OECD, 2004), in the absence and presence of food, for a period of 48 h. Neonates <24 h old were exposed to different concentrations of GDN (1.56, 3.13, 6.25, 12.5, 25, and 50 mg/L) and TBZ (0.16, 0.31, 0.63, 1.3, 2.5, and 5 mg/L). Five replicates with five neonates per replicate were exposed for each treatment plus controls. Whenever TBZ was assessed, a DMSO solvent control was incorporated. All toxicity experiments were initiated with neonates from the third to the fifth broods. For acute tests where food was provided, an initial suspension of 3×10^5 cell/mL of *R. subcapitata* was added. No additional food was provided until the end of each test. After 24 h and 48 h of exposure the number of immobilized daphnids was recorded by gently agitating the test vial and observing if swimming movements were or not visible. At the end of the tests pH and dissolved oxygen were checked to ensure the validity of the tests. The sensitivity of the daphnids was previously assessed by exposure to the reference substance, potassium dichromate, following OECD 202 guideline (OECD, 2004).

Algal toxicity tests were also performed. This assay provided information on chemicals' effects on *R. subcapitata*, as it was important to understand if the concentrations used were enough to induce already effects at the algae level, which was provided as food. *R. subcapitata* was routinely cultured using standard algal culture medium (pH 8.2) at 23 ± 1 °C under continuous illumination for 72 h (OECD, 2011). Algal cells were exposed to different concentrations of GDN (0.78, 1.56, 3.13, 6.25, 12.5, and 25 mg/L) and TBZ (0.16, 0.31, 0.63, 1.3, 2.5, 5, 10, and 20 mg/L). Controls containing DMSO at the same concentration were also tested and the concentration of DMSO was in all cases <0.1 mL/L (OECD, 2000). Growth experiments were performed with six replicates per sample. Biomass growth was estimated by measuring Optical Density at 750 nm (OD_{750nm}). The potential shading effect of GDN suspensions was investigated by placing 25 mL Erlenmeyer flaks with cultures of *R. subcapitata* cells (initial OD_{750nm} 0.1) into 100 mL beakers containing GDN suspensions (1.56, 3.13, 6.25, 12.5, and 25 mg/L) in OECD culture medium. The arrangement avoided direct contact between GDN suspensions and cells. The contribution of shading effect to algal growth inhibition was expressed as percentage with respect to experiments without GDN in the outer beaker.

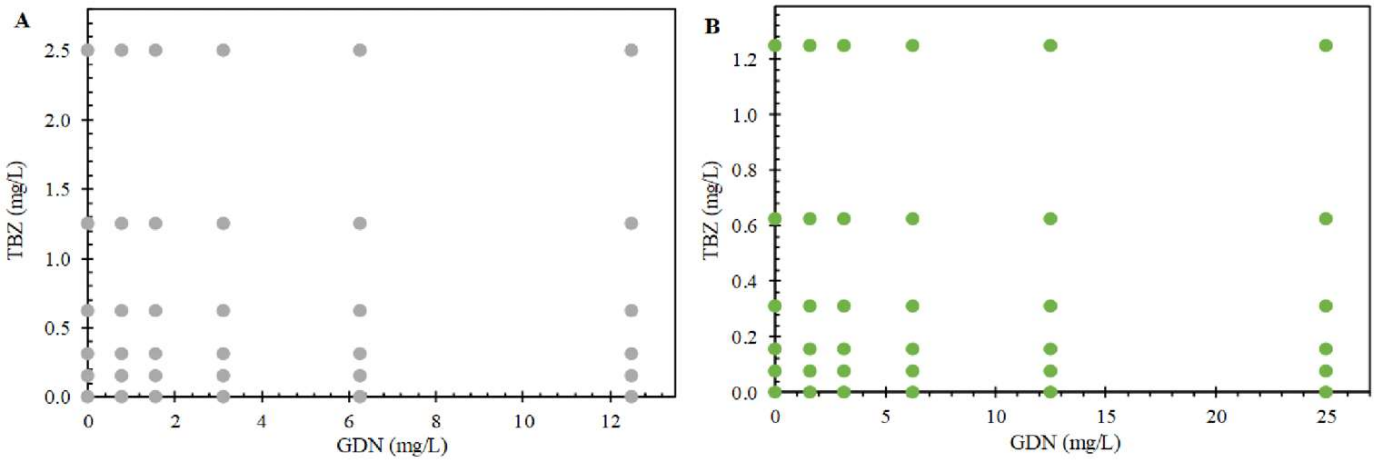

Figure 1. Experimental design of the combinations used for GDN-TBZ mixtures exposure to *Daphnia magna* in the absence (A), and in the presence of food (B).

2.3. Mixture toxicity assays

The toxic interactions of GDN-TBZ mixtures were studied using two sets of experiments, in the presence and absence of food (the microalga *R. subcapitata*). The experimental design follows a full factorial design and is presented in Fig. 1. In the absence of food, the concentrations ranged from 0.78 to 12.5 mg/L for GDN and from 0.16 to 2.5 mg/L for TBZ (Fig. 1 A). In the presence of food, mixtures concentrations ranged from 1.56 to 25 mg/L for GDN and from 0.08 to 1.25 mg/L for TBZ (Fig. 1 B). The concentrations of each compound in the binary mixtures were chosen based on their EC_{50} values from the single exposures for each experimental setup. Controls containing ASTM medium and DMSO solvent control were also included.

2.4. Data analysis

Data were statistically examined by means of R software 3.5.0 (The R Foundation for Statistical Computing©) and Rcmdr 2.5–1 package (Fox, 2005). The comparison between different treatments was performed by means of one-way analysis of variance (ANOVA) coupled with Tukey's HSD (honestly significant difference) post-hoc tests. Differences were considered statistically significant if $p < 0.05$. Dose-response curves of GDN and TBZ were fitted to the four-parameter log-logistic model (LL.4, drc) (Ritz et al., 2015). EC_{50} (effective concentration that causes 50% of growth inhibition or immobilization with respect to a non-treated control) values of GDN and TBZ, and confidence intervals were computed using the function ED.drc 3.0-1 (drc) (Ritz and Streibig, 2005). No significant differences were detected between organisms exposed to negative and solvent controls.

For predicting mixture toxicity, data were analysed using the MIXTOX tool (Jonker et al., 2005), using the reference models CA and IA. The deviations from CA and IA were modelled for synergism, antagonism, dose ratio (DR) and dose level (DL) dependencies, and computed using two parameters, *a* and *b*, forming a nested framework. The value of *a* indicates synergism ($a < 0$) or antagonism ($a > 0$) both for CA and IA. The parameter b_i describes deviations that depend on DR and quantifies the degree of antagonism ($b_i > 0$) or synergism ($b_i < 0$) due to the dominant compound. For DL dependency, a third parameter b_{DL} indicates the dose level at which synergism changes to antagonism or

Table 1. Interpretation of the parameters defining the functional form of deviation from CA and IA models; adapted from Jonker et al. (2005).

Deviation pattern	Parameter *a* (CA and IA)	Parameter *b* (CA)	Parameter *b* (IA)
Synergism/antagonism (S/A)	$a > 0$: antagonism $a < 0$: synergism	-	-
Dose ratio dependency (DR)	$a > 0$: antagonism except for those mixture ratios where negative *b* value indicates synergism $a < 0$: synergism except for those mixture ratios where positive *b* value indicates antagonism	$b_i > 0$: antagonism where the toxicity of the mixture is caused mainly by toxicant *i* $b_i < 0$: synergism where the toxicity of the mixture is caused mainly by toxicant *i*	
Dose level dependency (DL)	$a > 0$: antagonism at low dose level and synergism at high dose level $a < 0$: synergism at low dose level and antagonism at high dose level	$b_{DL} > 1$: change at lower EC_{50} level $b_{DL} = 1$: change at EC_{50} level $0 < b_{DL} < 1$: change at higher EC_{50} level $b_{DL} < 0$: no change but the magnitude of S/A is DL dependent	$b_{DL} > 2$: change at lower EC_{50} level $b_{DL} = 2$: change at EC_{50} level $1 < b_{DL} < 2$: change at higher EC_{50} level $b_{DL} < 1$: no change but the magnitude of S/A is effect level dependent

vice versa. A detailed description can be found elsewhere (Jonker et al., 2005). Within each conceptual model, data were fitted to the models and potential deviations and compared using the maximum likelihood method. When a significant deviation was identified, the mathematical parameters *a* and *b* were converted into biological effects as traduced in Table 1. In addition, the additivity of GDN-TBZ mixtures was assessed using the CI-isobologram method (Chou and Talalay, 1984). Additional details are provided as Supplementary Material (SM). Data analysis was performed by means of the computer program CompuSyn (Chou, 2006).

3. Results and discussion

3.1. Characterization of nanoparticle suspensions

Particle size and ζ-potential of GDN suspensions in ultrapure water, OECD algal culture medium and ASTM hard water medium (pH 8.0 ± 0.1) are shown in Table S1 (SM). The concentration of 10 mg/L was chosen based on the toxicity endpoints obtained for *D. magna* as shown in Table S2 (SM). DLS measurements revealed a tendency of GDN suspensions to aggregate/agglomerate, with mean sizes similar for all assayed media. The sizes of the background colloids (191 ± 17 nm for OECD medium and 165 ± 12 nm for ASTM medium) suggested heteroaggregation/agglomeration of GDN with culture media particles. ζ-potential values were negative in all cases and fall outside the stable range (<−30 mV or >+30 mV) indicative of non-stable suspensions. The TEM images shown in Fig. S1 (SM) confirmed the presence of aggregates/agglomerates of several hundreds of nanometers formed by primary particles of 3–4 nm.

3.2. Effect of GDN and TBZ on algal growth

The toxicity of GDN and TBZ to *R. subcapitata* was studied by tracking growth inhibition during 72 h tests. The dose-response curves are shown in Fig. S2 (SM). The EC_{50} value obtained for GDN was 5.5 ± 0.3 mg/L (EC_{20} 1.6 ± 0.2 mg/L, Table S2, SM). To our knowledge no previous data have been reported on GDN toxicity to *R. subcapitata*. We obtained EC_{50} values comparable with those of algae exposed to other carbon nanomaterials, which are generally in the lower tens of mg/L range (Long et al., 2012; Schwab et al., 2011). Somewhat higher toxicity was reported, however, for graphene oxide, with 72 h EC_{50} of 1.04 mg/L for the growth inhibition of *Chlamydomonas reinhardtii* (Martín-de-Lucía et al., 2018). As other carbon-based materials, GDN suspensions absorb visible light and can limit the light available for algal cells, which may result in growth inhibition (Baun et al., 2008; Wei et al., 2010). The capacity of GDN suspensions to physically block light and, consequently, to impair algal growth even in the absence of any direct contact between cells and nanoparticles, was assayed by conducting shading experiments (Hu et al., 2018). The comparison between cultures grown behind GDN suspensions and control cultures allowed calculating the influence of shading to *R. subcapitata* growth. The results are presented in Fig. S3 (SM). No significant ($p < 0.05$) 72 h growth inhibition was observed due to shading for concentrations up to 25 mg/L meaning that shading played a very minor impact on algal growth. Similar particles displayed toxic effects to *R. subcapitata* due to the overproduction of reactive oxygen species (ROS), which eventually induce lipid peroxidation and the disruption of cell envelopes, among other toxic effects (Nogueira et al., 2015).

Fig. S4 (SM) shows optical micrographs of daphnids after 48 h exposure to different GDN concentrations. The images demonstrated the accumulation of GDN within the gastrointestinal tract of daphnids as well as particle adhesion to their body surface. At the lower tested concentration, 3.13 mg/L, GDN was preferentially ingested by the daphnids. At higher GDN concentrations, the images showed considerable amount of nanoparticle aggregates adhered to the exoskeleton of daphnids covering their antennae and carapace with similar pattern either in the absence or in the presence of food. The toxic effect can be attributed at least in part to the limitation of the normal physiological activities of daphnids, such as swimming, filtering and moulting behaviour due to GDN aggregates.

The effect of TBZ to *R. subcapitata* growth is also shown in Table S2 (SM). EC_{50} for 72 h growth inhibition was 4.5 ± 0.5 mg/L, similar to the 96 h EC_{50} of 9 mg/L reported elsewhere (EU, 2001). Overall, our results indicated that the toxicity of GDN and TBZ for *R. subcapitata* growth was the same order as that observed for *D. magna*immobilization. The results showed that upon exposure concentrations algal growth rate was still positive after 72 h exposed to the EC_{50} values obtained for 48 h *D. magna* immobilization tests. This means that in joint exposure experiments using algae to feed daphnids, algal cells were still growing and serving their role as food source.

3.3. Toxicity of GDN to *D. magna*

Fig. 2 shows the results of the immobilization tests of *D. magna* neonates exposed to GDN in the absence and presence of food after 24 h and 48 h. After 24 h, no significant ($p < 0.01$) differences were obtained between exposure in the absence and presence of food (Fig. 2 A). After 48 h of exposure, and in the absence of food, the immobilization of daphnids was significantly ($p > 0.001$) higher than controls for concentrations ≥6.25 mg/L. *D. magna* immobilization was also significantly ($p < 0.001$) higher in the absence of food

than in assays performed in the presence of *R. subcapitata*. Fig. 2 B also shows that the differences between absence and presence of food were higher in 48 h immobilization assays with respect to 24 h data for the experiments performed at 6.25, 12.5 and 25 mg/L. This is a consequence of the higher resolution of 48 h tests at intermediate concentration of toxicants. The EC_{50}values for 48 h *D. magna* immobilization were 7.8 ± 0.3 mg/L (absence of food) and 18.9 ± 0.4 mg/L (in the presence of *R. subcapitata*). The EC_{20} values and the results for 24 h exposure are included in Table S2 (SM).

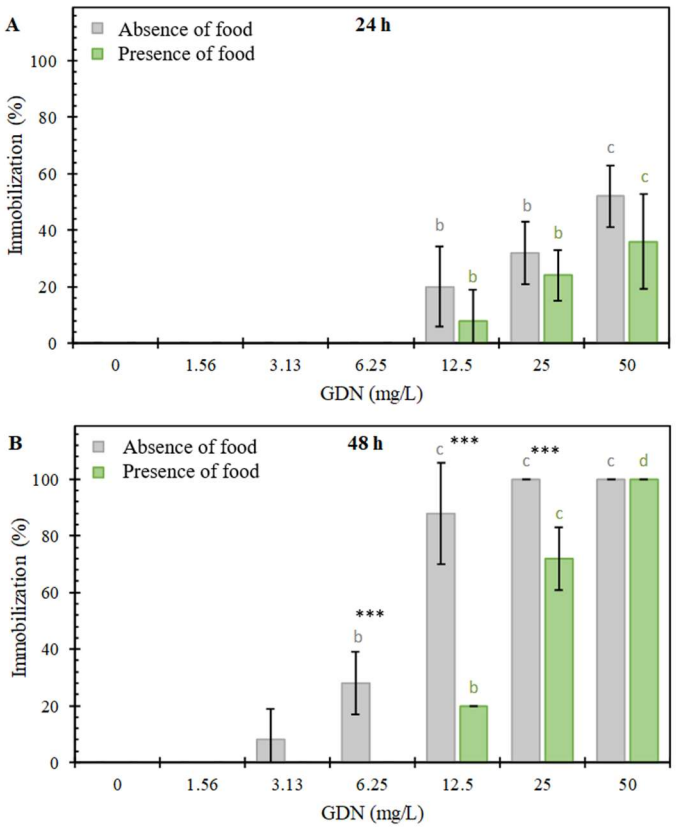

Figure 2. Effect of GDN, in the absence (grey bars) and presence (green bars) of food (*R. subcapitata*), on the immobilization of *D. magna* after 24 h (A) and 48 h (B) (error bars represent standard deviation, n = 5). Treatments with different letters are significantly different from controls (Tukey's HSD, $p < 0.01$). Asterisks indicate significant differences between groups ($p < 0.001$).

The toxicity of different carbon nanoparticles to *D. magna* has been widely reported in the literature with values generally coincident with this study. Sanchís et al. obtained 48 h EC_{50} values of 11, 14 and 20 mg/L for fullerene soot, multiwalled carbon nanotubes (MWCNT) and graphene, respectively (Sanchís et al., 2016). Zhu et al. found 48 h EC_{50} values of 8.7 mg/L for MWCNT (Zhu et al., 2009). In another study, it was reported that polyallylamine nanodiamonds and oxidized nanodiamonds induced the production of ROS in *D. magna* (Domínguez et al., 2018). Due to their hydrophobic properties, GDN aggregates may adhere to the carapaces of *D. magna*, which results in abnormal swimming behaviour and difficulties to moult (Mendonça et al., 2011; Nasser et al., 2016).

The toxicity of GDN to *D. magna* decreased in the presence of *R. subcapitata*. A similar behaviour was observed before for *D. magna* exposed to silver nanoparticles in the presence and absence of food (Allen et al., 2010; Mackevica et al., 2015; Ribeiro et al., 2014). The lower toxic damage could be attributed to the reduced bioavailability of GDN particles due to their heteroaggregation with organic matter and food residues (Allen et al., 2010). The relative instability of GDN suspensions as revealed by ζ-potential supports this hypothesis (Table S1). Heteroaggregation has been shown to dominate the interactions between nanoparticles and colloids, including biocolloids through different kind of electrostatic and non-electrostatic interactions (Wang et al., 2015). Heteroaggregation would be favoured by the ability of *R. subcapitata* to produce exudates that facilitate GDN aggregation (Koukal et al., 2007). We also observed daphnids with black particles adhered to their carapaces for high exposure concentrations (Fig. S4, SM). Accordingly, mechanical effects due to particle adherence may also be responsible for daphnids impairment. Finally, the higher toxicity observed in the absence of food could be related to the increased filtration rate of non-fed daphnids (Lampert, 1994; Plath, 1998).

3.4. Toxicity of TBZ to *D. magna*

The results of *D. magna* immobilization after exposure to TBZ in the absence and presence of *R. subcapitata* are shown in Fig. 3. After 24 h exposure, the immobilization of *D. magna* significantly ($p < 0.001$) increased for concentrations above 2.5 mg/L, remaining slightly below 50% even for the highest tested concentration (5 mg/L). No differences were found between feeding regimes after 24 h of exposure to TBZ (Fig. 3 A). For 48 h exposure, *D. magna* immobilization was considerably higher with significant ($p < 0.001$) differences between both feeding regimes observed for 0.63 and 1.25 mg TBZ/mL (Fig. 3 B). The EC_{50} of TBZ for 48 h exposure to *D. magna* was 0.55 ± 0.02 in the absence of food (Table S2, SM). These results agreed with the previously reported 48 h EC_{50} 0.85 mg/L (Oh et al., 2006). It has been shown that TBZ inhibits the activity of the mitochondrial enzyme fumarate reductase activity, thereby impairing mitochondrial respiration (Criado-Fornelio et al., 1987). Other compounds similar to TBZ also display high toxicity: benzimidazole, fenbendazole and flubendazole exhibit EC_{50} values of 0.017 mg/L, 0.019 mg/L, and 0.045–0.067 mg/L respectively (Oh et al., 2006; Wagil et al., 2015).

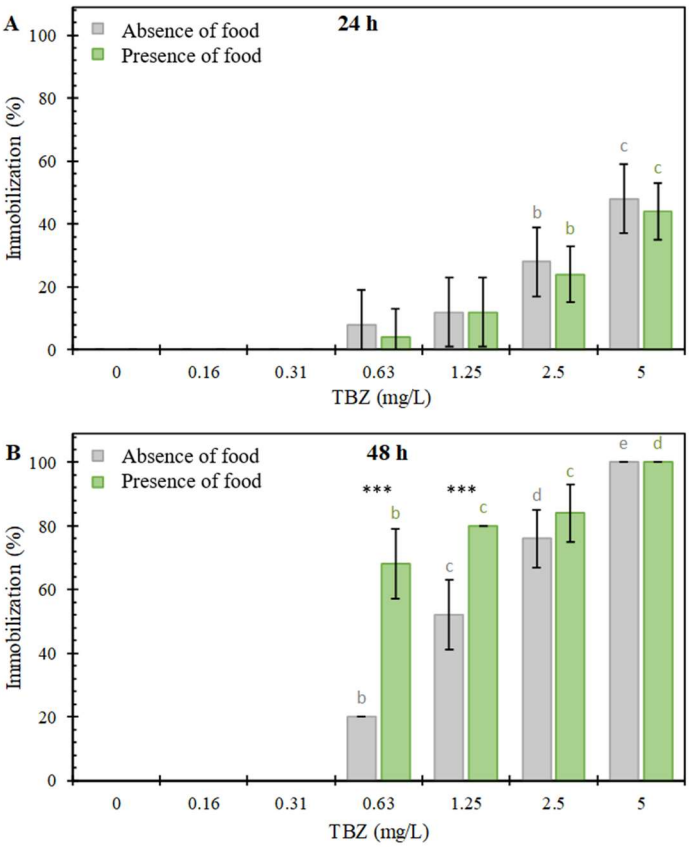

Figure 3. Effects of TBZ, in the absence (grey bars) and presence (green bars) of food (*R. subcapitata*), on the immobilization of *D. magna* after 24 h (A) and 48 h (B) (error bars represent standard deviation, n = 5). Treatments with different letters are significantly different from controls (Tukey's HSD, $p < 0.001$). Asterisks indicate significant differences between groups ($p < 0.001$).

The results showed that the toxicity of TBZ to *D. magna* increased in the presence of *R. subcapitata*, contrary to what was observed for GDN. TBZ is a weak base with pK_avalues of 4.17 (imidazole nitrogen) and ~2.5 (thiazolyl nitrogen). It is non-charged at neutral pH and is hydrophobic (log K_{OW} 2.47) with affinity to the non-polar moieties of organic matter. Accordingly, strong adsorption of TBZ on soil organic matter has been reported (Cayley and Lord, 1980). Once ingested, TBZ would become bioavailable in the gut of daphnids. Our results suggested that food may be an important pathway for trophic transfer of TBZ in *D. magna*. Several studies showed an increase of chemical toxicity to cladocerans in the presence of food. Lessard and Frost reported a higher toxicity of the Monsanto's glyphosate-based herbicide Roundup WeatherMax when supplied with phosphorous-rich diets (Lessard and Frost, 2012). Similarly, the antidepressant fluoxetine was found more toxic to *D. magna* in the presence of algal food (Hansen et al., 2008). Rose et al. reported the hydrophobic insecticide fenoxycarb adsorbed on algae resulting in increased toxicity to *Ceriodaphnia* cf. *dubia* when supplied with food (Rose et al., 2002).

3.5. Toxicity of GDN-TBZ mixtures to *D. magna*

The immobilization of *D. magna* exposed to GDN-TBZ mixtures in the absence and presence of food are shown in Fig. 4, Fig. 5, respectively. To quantify the combined toxicity of GDN and TBZ, both CA and IA were tested as reference conceptual models for mixture toxicity. Tables S3 and S4 (SM) show the values for the sum of squared residuals, SS, p-values for the conceptual model and the likelihood ratio test, $p(\chi 2)$, which quantifies the model's goodness of-fit, comparing the conceptual models and deviations. The individual EC_{50} values of GDN in the absence of food (8.9 mg/L for CA and 7.9 mg/L for IA, Table S3), and presence of food (21.6 mg/L for CA and 20.4 mg/L for IA, Table S4) obtained from the single exposures within this mixture experimental setup agree well with the EC_{50} values obtained from the exposures to single toxicants (7.8 mg/L and 18.9 mg/L, as indicated in Table S2). Predicted EC_{50} values for TBZ in were 0.69 mg/L (CA) and 0.52 mg/L (IA) in the absence of food, and 0.78 (CA) and 0.71 (IA) in the presence of food, also similar to the results obtained in single exposure experiments: 1.3 mg/L and 0.55 mg/L respectively (Table S2).

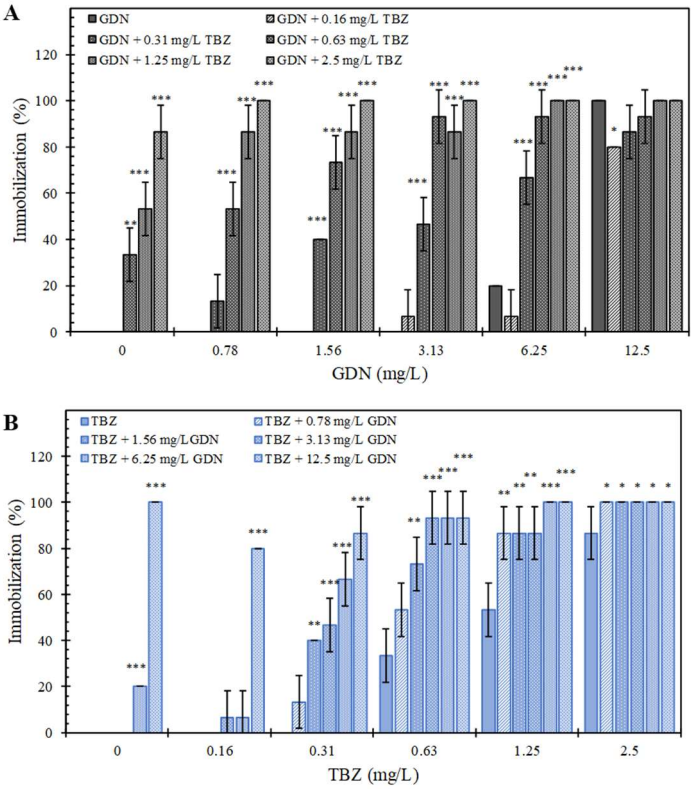

Figure 4. Effects of the binary mixtures of GDN (A) and TBZ (B) on the immobilization of *D. magna* in the absence of food (*R. subcapitata*). (Error bars represent standard deviation, n = 3; asterisks indicate significant differences with control, $p < 0.05$).

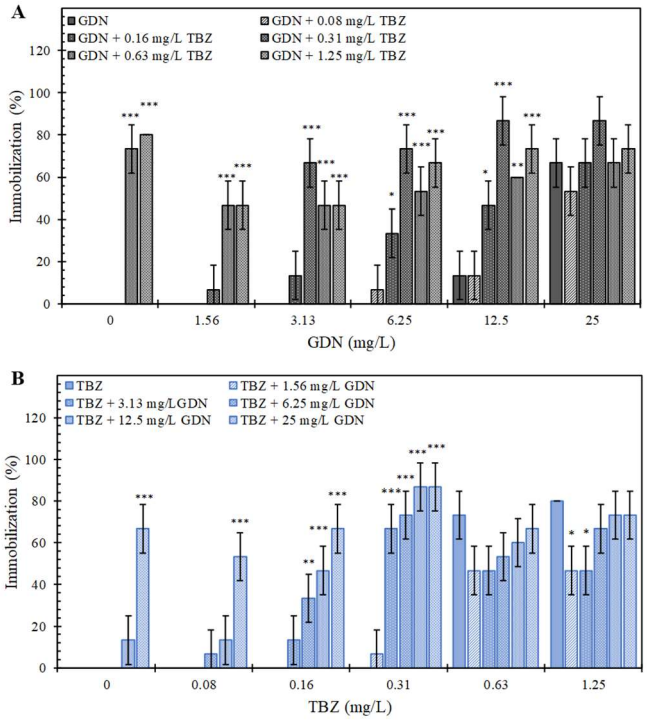

Figure 5. Effect of the binary mixtures of GDN (A) and TBZ (B) on the immobilization of *D. magna* in the presence of food (*R. subcapitata*). (Error bars represent standard deviation, n = 3; asterisks indicate significant differences with control, $p < 0.05$).

In all cases, the combined toxicity of GDN and TBZ mixtures fitted better to CA model (Tables S3 and S4) in the sense that CA model explained a higher proportion of the total variance. The results in the absence of food fitted better to DR dependency with $a < 0$ and $b > 0$ (Table 1), which represent dose ratio deviation with synergism except for dose ratios in which toxicity was dominated by one toxicant (Fig. 6 C and D). The isobolograms (Fig. 6 C and D) showed clear synergism at low dose levels moving towards antagonism for increasing GDN doses. In experiments using daphnids fed with *R. subcapitata*, the DL dependency of CA model explained a higher proportion of variance ($a < 0$ and $b_{DL} > 0$, Tables 1 and S4), indicating synergism at low dose levels changing to antagonism at higher doses, again a result observed in the isobolograms of Fig. 7. The tendency to antagonism was also clear for doses higher than mixture EC_{50} (A brief explanation about isobologram plots is included as Supplementary Material).

We also used CI-isobologram method as complementary methodology to check the nature of GDN-TBZ toxicological interactions. CI provides a unique parameter to quantify the degree of synergism or antagonism as a function of the degree of immobilization or affected fraction, f_a. Fig. 8 shows the

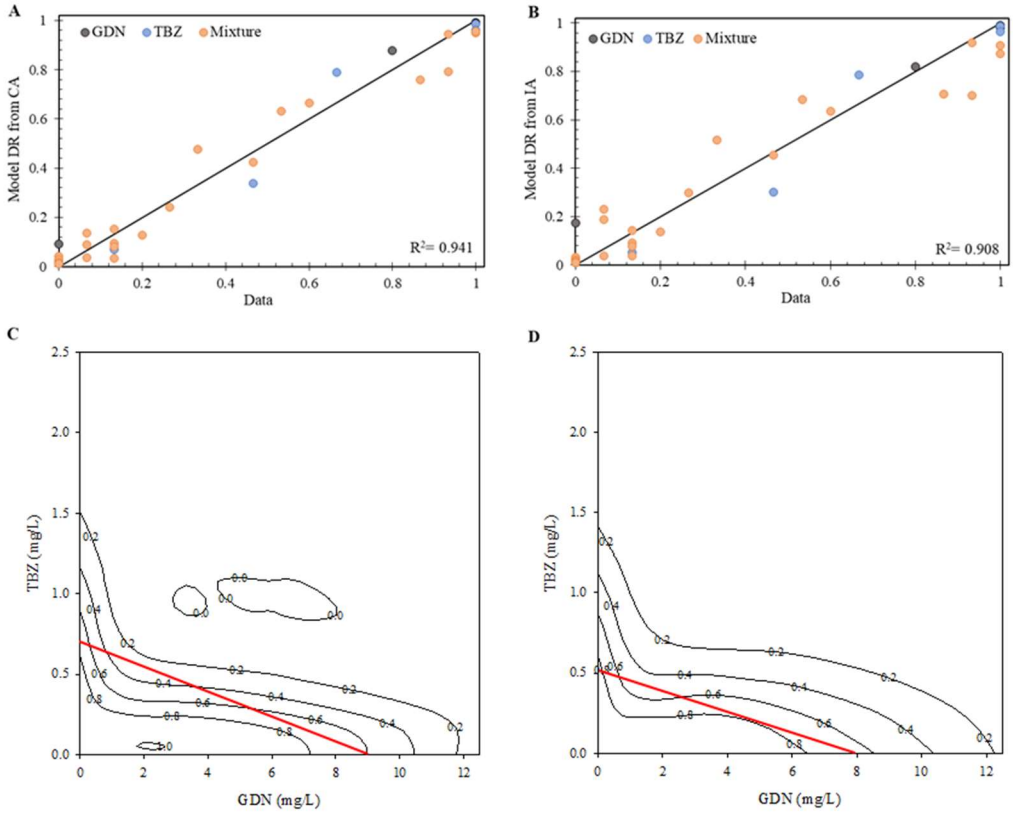

Figure. 6. Effects of GDN-TBZ mixtures in the absence of food (*R. subcapitata*) on *D. magna* immobilization. Relationship between observed data and modelled values for CA-DR (A) and IA-DR (B). Isobolograms representing the response surfaces for DR deviation from CA (C) and IA (D) models. TU = 1 additivity line (-, red). (The numbers indicate the response level).

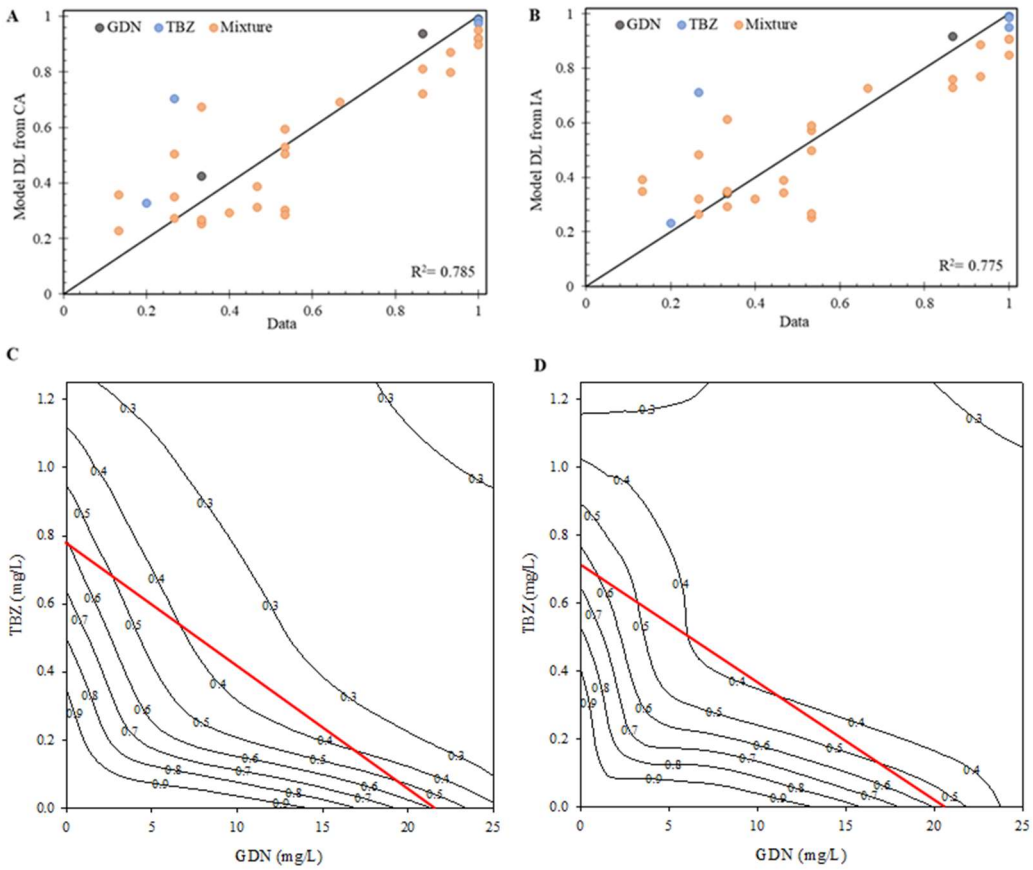

Figure. 7. Effects of GDN-TBZ mixtures in the presence of food (*R. subcapitata*) on *D. magna* immobilization. Relationship between observed data and modelled values for CA-DL (A) and IA-DL (B). Isobolograms representing the response surfaces for DL deviation from CA (C) and IA (D) models. TU = 1 additivity line (-, red).

affected fraction (f_a)-CI plots for the binary GDN-TBZ combinations in the presence and absence of food. The pattern was similar for both feeding conditions. GDN-TBZ combinations displayed synergism for $f_a > 0.1$ with a slight tendency to additivity for the higher affected fractions in the experiments performed in the absence of food. The synergism was clear in all cases within the $0.1 < f_a < 0.8$ range and higher (lower CI) in the presence of food. Table S5 (SM) shows the fitting parameters (EC_{50}, m, and r) of GDN, TBZ and their binary mixtures. In all cases the shape of the dose-effect curves was sigmoidal and good fit was obtained indicating conformity to the median-effect principle (see SM for details).

In this study, we have shown that low-to-intermediate concentrations of GDN and TBZ were associated to a synergistic toxic response of *D. magna* to their binary combinations. Synergism might be explained considering GND acted as vehicle to increase the exposure to TBZ. The interaction between the aromatic molecule TBZ and the graphitic surface of GDN could be attributed to the formation of π-stacked complexes in which TBZ molecules interact with the sp^2-like surface of GDN (Rochefort and Wuest, 2009). To verify the adsorption hypothesis, we performed ATR-FTIR spectra of GDN kept 24 h in contact with TBZ with the proportion of their respective EC_{50} concentrations,

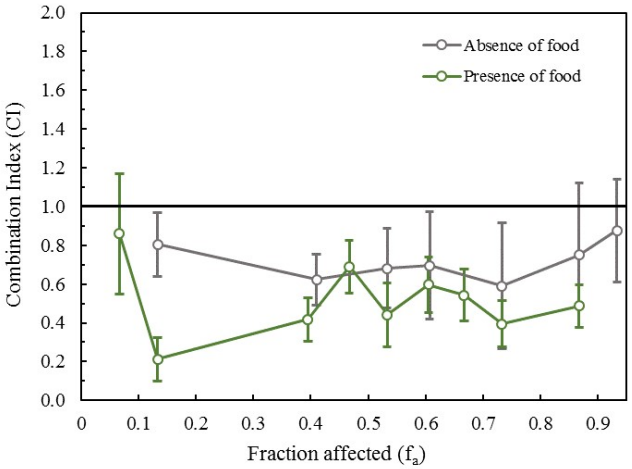

Figure 8. Combination index (CI-f_a) plot for GDN-TBZ binary combinations in the presence (green) and absence (grey) of food (*R. subcapitata*). CI > 1 indicates antagonism, CI < 1 indicates synergism and C = 1 represents additivity. Error bars represent standard deviation.

centrifuged, washed and dried before being analysed. The bands corresponding to the characteristics features of TBZ were observed in the spectrum of recovered GDN as indicated in Fig. S5 (SM).

When GDN is present at higher concentrations it induces antagonism, which could be explained by particle agglomeration to such an extent that the mixture becomes less available. A similar antagonistic behaviour of in mixtures of pollutants with graphene oxide was described elsewhere and attributed to a reduced bioavailability of pollutants and nanoparticles because of particle aggregation/agglomeration (Martín-de-Lucía et al., 2018). The presence of *R. subcapitata* as food source reduced toxicity and synergism, which was probably due to the adsorption of GDN and TBZ onto aggregates with algal cells.

The toxicity enhancement due to the combination of toxic chemicals with carbon-based nanomaterials has been described before and is expected to be particularly important for filter feeding organisms like *D. magna*. Baun et al. and *Zindler* et al. reported higher toxicity of phenanthrene in the presence of C_{60} nanoparticles and CNT for the immobilization of *D. magna* (Baun et al., 2008; Zindler et al., 2016). Synergism was also reported for *D. magna* exposed to a combination of fullerenes and malathion (Sanchís et al., 2016). Synergistic toxic effects were also observed for metals: CNT and C_{60} increased the toxicity of cadmium, copper and arsenic to *D. magna* (Tao et al., 2013; Wang et al., 2016a; Wang et al., 2016b).

The antagonistic response of mixtures containing nanoparticles at high concentrations due particle aggregation and sedimentation was also observed before (Baun et al., 2008; Simon et al., 2015). Our results showed that non-additive interactions existed at all toxic levels when exposing *D. magna* to mixtures of GDN and TBZ. Also, the sign and intensity of the interaction depends on the dose of the mixture. The consequences of non-additivity have been largely ignored, but the limits of the additivity paradigm pose a significant challenge for regulatory frameworks.

Conclusions

The EC_{50} for the 48-h immobilization of *D. magna* exposed to GDN was 7.8 mg/L in the absence of *R. subcapitata* as food source and 18.9 mg/L in the presence of food. The presence of the micro green algae *R. subcapitata* mitigated the toxicity of GDN, but increased the toxicity of TBZ, with the EC_{50} decreasing from 1.3 mg/L to 0.55 mg/L, suggesting a carrier effect for TBZ.

The results from the binary mixtures of GDN and TBZ showed synergistic toxic interactions at low concentrations, probably because GDN increases the bioavailability of TBZ. At high GDN doses, an antagonistic effect was observed, which was attributed to the formation of aggregates of GDN eventually reducing the bioavailability of TBZ.

The non-additive effects observed for the binary mixtures between GDN and TBZ along a wide range of concentrations and affected fractions, proved the limits of the additivity paradigm. Our findings showed the importance of considering toxicological interactions and the interaction with other organisms in trophic chains for realistic toxicity assessment.

Acknowledgements

Thanks are due for the financial support to CESAM (UID/AMB/50017/2019), to FCT/MEC through national funds. The authors also thank the Spanish Ministry of Science, CTM2016-74927-C2-1-R/2-R. IML thanks the Spanish Ministry of Science and the European Union for the award of a FPI contract (BES-2014-070093).

References

Allen HJ, Impellitteri CA, Macke DA, Heckman JL, Poynton HC, Lazorchak JM, et al. Effects from filtration, capping agents, and presence/absence of food on the toxicity of silver nanoparticles to *Daphnia magna*. Environ. Toxicol. Chem. 2010; 29: 2742-2750.

Antunes SC, Castro BB, Gonçalves F. Chronic responses of different clones of *Daphnia longispina* (field and ephippia) to different food levels. Acta Oecologica 2003; 24: S325-S332.

ASTM. E729-96 Standard guide for conducting acute toxicity tests on test materials with fishes, macroinvertebrates, and amphibians. ASTM International, West Conshohocken, PA, 2014.

Baun A, Sørensen SN, Rasmussen RF, Hartmann NB, Koch CB. Toxicity and bioaccumulation of xenobiotic organic compounds in the presence of aqueous suspensions of aggregates of nano-C_{60}. Aquat. Toxicol. 2008; 86: 379-387.

Bradac C, Osswald S. Effect of structure and composition of nanodiamond powders on thermal stability and oxidation kinetics. Carbon 2018; 132: 616-622.

Brown HD, Matzuk AR, Ilves IR, Peterson LH, Harris SA, Sarett LH, et al. Antiparasitic drugs. IV. 2-(4'thiazolyl)-benzimidazole, a new anthelmintic. J. Am. Chem. Soc. 1961; 83: 1764-1765.

Cayley GR, Lord KA. The extraction and assay of thiabendazole in strongly adsorbing soils. Pestic. Sci. 1980; 11: 9-14.

Ccanccapa A, Masiá A, Navarro-Ortega A, Picó Y, Barceló D. Pesticides in the Ebro River basin: Occurrence and risk assessment. Environ. Pollut. 2016; 211: 414-424.

Criado-Fornelio A, Rodríguez-Caabeiro F, Jiménez-González A. The mode of action of some benzimidazole drugs on *Trichinella spiralis*. Parasitology 1987; 95: 61-70.

Chou TC. Theoretical basis, experimental design, and computerized simulation of synergism and antagonism

in drug combination studies. Pharmacol. Rev. 2006; 58: 621-681.
Chou TC, Talalay P. Quantitative analysis of dose-effect relationships: the combined effects of multiple drugs or enzyme inhibitors. Adv. Enzyme. Regul. 1984; 22: 27-55.
De Volder MFL, Tawfick SH, Baughman RH, Hart AJ. Carbon nanotubes: present and future commercial applications. Science 2013; 339: 535-539.
Domínguez GA, Torelli MD, Buchman JT, Haynes CL, Hamers RJ, Klaper RD. Size dependent oxidative stress response of the gut of *Daphnia magna* to functionalized nanodiamond particles. Environ. Res. 2018; 167: 267-275.
EPA. Registration Eligibility Decision: Thiabendazole and salts. In: Agency USEP, editor. EPA-738-F-02-002, 2002.
EU. Review report for the active substance thiabendazole. In: Directorate E-Public AaPH, editor. European Commission, 2001.
EU. Toxicity and Assessment of Chemical Mixtures. In: Scientific Committee on Health and Environmental Risks (SCHER) SCoEaNIHRSaSCoCSS, editor. European Commission, Brussels 2012.
Fox J. Getting started with the R commander: a basic-statistics graphical user interface to R. Journal of Statistical Software 2005; 14: 1-42.
Godoy AA, Kummrow F. What do we know about the ecotoxicology of pharmaceutical and personal care product mixtures? A critical review. Crit. Rev. Environ. Sci. Technol. 2017; 47: 1453-1496.
Hansen LK, Frost PC, Larson JH, Metcalfe CD. Poor elemental food quality reduces the toxicity of fluoxetine on *Daphnia magna*. Aquat. Toxicol. 2008; 86: 99-103.
Hu J, Wang J, Liu S, Zhang Z, Zhang H, Cai X, et al. Effect of TiO_2 nanoparticle aggregation on marine microalgae *Isochrysis galbana*. J. Environ. Sci. 2018; 66: 208-215.
Jonker MJ, Svendsen C, Bedaux JJM, Bongers M, Kammenga JE. Significance testing of synergistic/antagonistic, dose level-dependent, or dose ratio-dependent effects in mixture dose-response analysis. Environ. Toxicol. Chem. 2005; 24: 2701-2713.
Jośko I, Oleszczuk P, Skwarek E. Toxicity of combined mixtures of nanoparticles to plants. J. Hazard. Mater. 2017; 331: 200-209.
Karpeta-Kaczmarek J, Kędziorski A, Augustyniak-Jabłokow MA, Dziewięcka M, Augustyniak M. Chronic toxicity of nanodiamonds can disturb development and reproduction of *Acheta domesticus* L. Environ. Res. 2018; 166: 602-609.
Koukal B, Rossé P, Reinhardt A, Ferrari B, Wilkinson KJ, Loizeau J-L, et al. Effect of *Pseudokirchneriella subcapitata* (Chlorophyceae) exudates on metal toxicity and colloid aggregation. Water Res. 2007; 41: 63-70.
Kumar S, Nehra M, Kedia D, Dilbaghi N, Tankeshwar K, Kim K-H. Nanodiamonds: Emerging face of future nanotechnology. Carbon 2019; 143: 678-699.
Lampert W. Phenotypic plasticity of the filter screens in *Daphnia*: Adaptation to a low-food environment. Limnol. Oceanogr. 1994; 39: 997-1006.
Lessard CR, Frost PC. Phosphorus nutrition alters herbicide toxicity on *Daphnia magna*. Sci. Total Environ. 2012; 421-422: 124-128.
Long Z, Ji J, Yang K, Lin D, Wu F. Systematic and quantitative investigation of the mechanism of carbon nanotubes toxicity toward algae. Environ. Sci. Technol. 2012; 46: 8458-8466.
Lopes S, Pinheiro C, Soares AMVM, Loureiro S. Joint toxicity prediction of nanoparticles and ionic counterparts: Simulating toxicity under a fate scenario. J. Hazard. Mater. 2016; 320: 1-9.
Loureiro S, Svendsen C, Ferreira ALG, Pinheiro C, Ribeiro F, Soares AMVM. Toxicity of three binary mixtures to *Daphnia magna*: Comparing chemical modes of action and deviations from conceptual models. Environ. Toxicol. Chem. 2010; 29: 1716-1726.
Mackevica A, Skjolding LM, Gergs A, Palmqvist A, Baun A. Chronic toxicity of silver nanoparticles to *Daphnia magna* under different feeding conditions. Aquat. Toxicol. 2015; 161: 10-16.
Martín-de-Lucía I, Campos-Mañas MC, Agüera A, Leganés F, Fernández-Piñas F, Rosal R. Combined toxicity of graphene oxide and wastewater to the green alga *Chlamydomonas reinhardtii*. Environ. Sci. Nano 2018; 5: 1729-1744.
Martín-de-Lucía I, Campos-Mañas MC, Agüera A, Rodea-Palomares I, Pulido-Reyes G, Leganés F, et al. Reverse Trojan-horse effect decreased wastewater toxicity in the presence of inorganic nanoparticles. Environ. Sci. Nano 2017; 4: 1273-1282.
Mendonça E, Diniz M, Silva L, Peres I, Castro L, Correia JB, et al. Effects of diamond nanoparticle exposure on the internal structure and reproduction of *Daphnia magna*. J. Hazard. Mater. 2011; 186: 265-271.
Mochalin VN, Shenderova O, Ho D, Gogotsi Y. The properties and applications of nanodiamonds. Nature Nanotechnology 2011; 7: 11.
Mundra RV, Wu X, Sauer J, Dordick JS, Kane RS. Nanotubes in biological applications. Curr. Opin. Biotechnol. 2014; 28: 25-32.
Nasser F, Davis A, Valsami-Jones E, Lynch I. Shape and charge of gold nanomaterials influence survivorship, oxidative stress and moulting of *Daphnia magna*. Nanomaterials 2016; 6: 222.
Nian Q, Wang Y, Yang Y, Li J, Zhang MY, Shao J, et al. Direct laser writing of nanodiamond films from graphite under ambient conditions. Sci. Rep. 2014; 4: 6612.
Nogueira PFM, Nakabayashi D, Zucolotto V. The effects of graphene oxide on green algae *Raphidocelis subcapitata*. Aquat. Toxicol. 2015; 166: 29-35.
OECD. Guidance document on aquatic toxicity testing of difficult substances and mixtures. OECD Series on Testing and Assessment. 23. OECD Publishing, Paris, 2000.
OECD. Test No. 202: *Daphnia* sp. Acute immobilisation test. OECD Guidelines for Testing of Chemicals. OECD Publishing, Paris, 2004.
OECD. Test No. 201: Freshwater alga and cyanobacteria, growth inhibition test. OECD Guidelines for Testing of Chemicals. OECD Publishing, Paris, 2011.
Oh SJ, Park J, Lee MJ, Park SY, Lee J-H, Choi K. Ecological hazard assessment of major veterinary benzimidazoles:

Acute and chronic toxicities to aquatic microbes and invertebrates. Environ. Toxicol. Chem. 2006; 25: 2221-2226.
Pereira JL, Gonçalves F. Effects of food availability on the acute and chronic toxicity of the insecticide methomyl to *Daphnia* spp. Sci. Total Environ. 2007; 386: 9-20.
Pieters BJ, Liess M. Maternal nutritional state determines the sensitivity of *Daphnia magna* offspring to short-term fenvalerate exposure. Aquat. Toxicol. 2006; 76: 268-277.
Plath K. Adaptive feeding behavior of *Daphnia magna* in response to short-term starvation. Limnol. Oceanogr. 1998; 43: 593-599.
Ribeiro F, Gallego-Urrea JA, Jurkschat K, Crossley A, Hassellöv M, Taylor C, et al. Silver nanoparticles and silver nitrate induce high toxicity to *Pseudokirchneriella subcapitata*, *Daphnia magna* and *Danio rerio*. Sci. Total Environ. 2014; 466-467: 232-241.
Ritz C, Baty F, Streibig JC, Gerhard D. Dose-Response Analysis Using R. PLOS One 2015; 10: e0146021.
Ritz C, Streibig JC. Bioassay Analysis Using R. J. Stat. Softw. 2005; 12: 22.
Robinson HJ, Silber RH, Graessle OE. Thiabendazole: toxicological, pharmacological and antifungal properties. Texas Reports on Biology and Medicine 1969; 27: Suppl 2:537+.
Rochefort A, Wuest JD. Interaction of substituted aromatic compounds with graphene. Langmuir 2009; 25: 210-215.
Rosal R, Rodea-Palomares I, Boltes K, Fernández-Piñas F, Leganés F, Petre A. Ecotoxicological assessment of surfactants in the aquatic environment: Combined toxicity of docusate sodium with chlorinated pollutants. Chemosphere 2010; 81: 288-293.
Rose RM, Warne MSJ, Lim RP. Food concentration affects the life history response of *Ceriodaphnia* cf. *dubia* to chemicals with different mechanisms of action. Ecotox. Environ. Saf. 2002; 51: 106-114.
Sanchís J, Olmos M, Vincent P, Farré M, Barceló D. New insights on the influence of organic co-contaminants on the aquatic toxicology of carbon nanomaterials. Environ. Sci. Technol. 2016; 50: 961-969.
Schrand AM, Hens SAC, Shenderova OA. Nanodiamond particles: Properties and perspectives for bioapplications. Crit. Rev. Solid State Mater. Sci. 2009; 34: 18-74.
Schwab F, Bucheli TD, Lukhele LP, Magrez A, Nowack B, Sigg L, et al. Are carbon nanotube effects on green algae caused by shading and agglomeration? Environ. Sci. Technol. 2011; 45: 6136-6144.
Silva E, Martins C, Pereira AS, Loureiro S, Cerejeira MJ. Toxicity prediction and assessment of an environmentally realistic pesticide mixture to *Daphnia magna* and *Raphidocelis subcapitata*. Ecotoxicology 2018; 27: 956-967.
Simon A, Preuss TG, Schäffer A, Hollert H, Maes HM. Population level effects of multiwalled carbon nanotubes in *Daphnia magna* exposed to pulses of triclocarban. Ecotoxicology 2015; 24: 1199-1212.
Tao X, He Y, Fortner JD, Chen Y, Hughes JB. Effects of aqueous stable fullerene nanocrystal (nC60) on copper (trace necessary nutrient metal): Enhanced toxicity and accumulation of copper in *Daphnia magna*. Chemosphere 2013; 92: 1245-1252.
Taylor G, Baird DJ, Soares AMVM. Surface binding of contaminants by algae: Consequences for lethal toxicity and feeding to *Daphnia magna* straus. Environ. Toxicol. Chem. 1998; 17: 412-419.
Tran NH, Reinhard M, Gin KY-H. Occurrence and fate of emerging contaminants in municipal wastewater treatment plants from different geographical regions-a review. Water Res. 2018; 133: 182-207.
van der Laan K, Hasani M, Zheng T, Schirhagl R. Nanodiamonds for *in vivo* applications. Small 2018; 14: 1703838.
Wagil M, Białk-Bielińska A, Puckowski A, Wychodnik K, Maszkowska J, Mulkiewicz E, et al. Toxicity of anthelmintic drugs (fenbendazole and flubendazole) to aquatic organisms. Environmental Science and Pollution Research 2015; 22: 2566-2573.
Wang H, Adeleye AS, Huang Y, Li F, Keller AA. Heteroaggregation of nanoparticles with biocolloids and geocolloids. Adv. Colloid Interface Sci. 2015; 226: 24-36.
Wang X, Qu R, Allam AA, Ajarem J, Wei Z, Wang Z. Impact of carbon nanotubes on the toxicity of inorganic arsenic [As(III) and As(V)] to *Daphnia magna*: The role of certain arsenic species. Environ. Toxicol. Chem. 2016a; 35: 1852-1859.
Wang X, Qu R, Liu J, Wei Z, Wang L, Yang S, et al. Effect of different carbon nanotubes on cadmium toxicity to *Daphnia magna*: The role of catalyst impurities and adsorption capacity. Environ. Pollut. 2016b; 208: 732-738.
Wei L, Thakkar M, Chen Y, Ntim SA, Mitra S, Zhang X. Cytotoxicity effects of water dispersible oxidized multiwalled carbon nanotubes on marine alga, *Dunaliella tertiolecta*. Aquat. Toxicol. 2010; 100: 194-201.
Wierzbicki M, Sawosz E, Grodzik M, Hotowy A, Prasek M, Jaworski S, et al. Carbon nanoparticles downregulate expression of basic fibroblast growth factor in the heart during embryogenesis. Int. J. Nanomed. 2013; 8: 3427-35.
Zakrzewska KE, Samluk A, Wierzbicki M, Jaworski S, Kutwin M, Sawosz E, et al. Analysis of the cytotoxicity of carbon-based nanoparticles, diamond and graphite, in human glioblastoma and hepatoma cell lines. PLOS One 2015; 10: e0122579-e0122579.
Zhu X, Zhu L, Chen Y, Tian S. Acute toxicities of six manufactured nanomaterial suspensions to *Daphnia magna*. J. Nanopart. Res. 2009; 11: 67-75.
Zindler F, Glomstad B, Altin D, Liu J, Jenssen BM, Booth AM. Phenanthrene bioavailability and toxicity to *Daphnia magna* in the presence of carbon nanotubes with different physicochemical properties. Environ. Sci. Technol. 2016; 50: 12446-12454.

SUPPLEMENTARY MATERIAL

Combined toxicity of graphite-diamond nanoparticles and thiabendazole to *Daphnia magna*

Idoia Martín-de-Lucía[1], Sandra F. Gonçalves[2], Francisco Leganés[3], Francisca Fernández-Piñas[3], RobertoRosal[1,*], SusanaLoureiro[2,*]

[1] Department of Chemical Engineering, University of Alcalá, E-28871 Alcalá de Henares, Madrid, Spain
[2] Department of Biology & CESAM, University of Aveiro, Campus Universitario de Santiago, 3810-193 Aveiro, Portugal
[3] Department of Biology, Universidad Autónoma de Madrid, E-28049 Madrid, Spain

[*] Corresponding authors: roberto.rosal@uah.es, sloureiro@ua.pt

Contents

Isobolograms and isoboles.

An isobologram is Cartesian coordinate plot displaying the combinations of individual doses that produce a certain joint effect at level "x" (For EC_{50}, x = 50 and so on). Every level of effect has an associated line termed isobole. (Tallarida et el. 2006). The isoboles serve as a visual guide to display additivity and non-additive behaviours. If, for a certain effect level, i.e. 50%, there is no toxic interaction between the two compounds, the isobole would be a straight line connecting the intercepts (doses). (See figure below.)

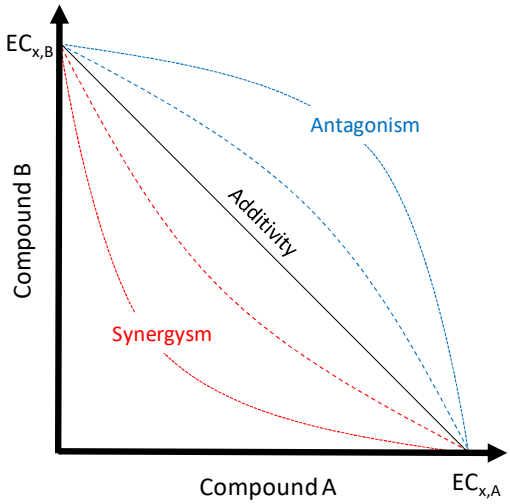

When the isobole lies below the additivity line (concave-up line), there is a synergistic behaviour. When the isobole lies above the additivity line (concave-down), the behaviour is antagonistic. Isoboles are generally, but not necessarily, based on the concentration-addition model. In fact, isoboles do not depend on mechanistic assumptions and are independent of the shapes of the dose-response curves so that they might apply for any model of additivity (Berenbaum, 1981).

Tallarida, R.J. An overview of drug combination analysis with isobolograms, Journal of Pharmacology and Experimental Therapeutics, 2006; 319: 1-7.

Berenbaum, M.C. Criteria for analyzing interactions between biologically active agents. Advances in Cancer Research, 1981: 35: 269-335.

Combination index (CI) for determining combined toxicity.

The response to combined toxicity tests was estimated using the median-effect equation (Chou and Talalay, 1984) based on the mass-action law:

$$\frac{fa}{fu} = \left(\frac{D}{Dm}\right)^m \quad (1)$$

where f_a is the fraction affected by a certain dose, D, expressed as concentration of toxicant, f_u is the unaffected fraction (f_a = 1 - f_u), D_m represents the dose for 50% effect (median effect-dose or EC_{50}), and m is the sigmoidicity coefficient of the dose-effect curve where m = 1, m > 1, and m < 1 indicate hyperbolic, sigmoidal, and negative sigmoidal dose-effect curve, respectively. Therefore, the method considers both potency (D_m) and shape (m) parameters. Eq. 1 may be arranged as follows:

$$D = D_m \left(\frac{fa}{1-fa}\right)^{1/m} \quad (2)$$

D_m and m values for individual GDN and TBZ and their binary mixtures were determined by fitting x = log (D) versus y = log (f_a/f_u). The conformity of the data to the median-effect principle can be assessed by the linear correlation coefficient (r). These parameters were then used to calculate doses of individual compounds and their combinations required to produce various effect levels. Combination index (CI) values for each effect level were calculated according to the general CI equation (Chou, 2006):

$$n_{(CI)_x} = \sum_{j=1}^{n} \frac{(D)_j}{(D_x)_j} = \sum_{j=1}^{n} \frac{(D_x)_{1-n}\left(\frac{[D]_j}{\sum_1^n [D]}\right)}{(D_m)_j\left(\frac{(fa_x)_j}{[1-(fa_x)_j]}\right)^{1/mj}} \quad (3)$$

where $_n(CI)_x$ is the combination index for n chemicals at x % immobilization; $(D_x)_{1-n}$ is the sum of the dose of n chemicals that exerts x % immobilization in combination, $([D]_j / \sum_1^n [D])$ is the proportionality of the dose of each of n chemicals that exerts x % immobilization in combination; and $(D_m)_j (fa_x)_j / [1 - (fa_x)_j]_{1/mj}$ is the dose of each drug alone that exerts x % immobilization. From Eq. 3, CI < 1, CI = 1 and CI > 1 indicates synergism, additive effect and antagonism, respectively (Chou, 2006).

References

Chou T-C, Talalay P. Quantitative analysis of dose-effect relationships: the combined effects of multiple drugs or enzyme inhibitors. Advances in Enzyme Regulation 1984; 22: 27-55.

Chou TC. Theoretical basis, experimental design, and computerized simulation of synergism and antagonism in drug combination studies. Pharmacol Rev 2006; 58: 621-81.

Table S1. Physicochemical properties of GDN suspensions (10 mg/L) in ultrapure water, OECD algal culture medium and ASTM hard water medium at different times (ζ-potential measured at pH 7.9-8.2).

	Ultrapure water			OECD medium*			ASTM medium**		
	d_{DLS} (nm)	PdI	ζ-potential (mV)	d_{DLS} (nm)	PdI	ζ-potential (mV)	d_{DLS} (nm)	PdI	ζ-potential (mV)
0 h	396 ± 25	0.27 ± 0.03	-5.4 ± 0.2	431 ± 10	0.24 ± 0.02	-2.5 ± 0.2	472 ± 41	0.15 ± 0.02	-5.8 ± 0.3
24 h	450 ± 10	0.39 ± 0.01	-7.8 ± 0.4	582 ± 58	0.33 ± 0.07	-3.5 ± 0.1	642 ± 47	0.27 ± 0.02	-7.2 ± 0.5
48 h	615 ± 24	0.26 ± 0.04	-8.2 ± 0.5	623 ± 62	0.25 ± 0.02	-5.9 ± 0.4	679 ± 58	0.26 ± 0.02	-8.8 ± 0.3
72 h	620 ± 21	0.37 ± 0.02	-12.2 ± 0.4	881 ± 56	0.36 ± 0.01	-6.1 ± 0.4	-	-	-

* OECD medium: d_{DLS} 191 ± 17 nm; ζ-potential -13.7 ± 0.8 mV.
** ASTM medium: d_{DLS} 165 ± 12 nm; ζ-potential -3.2 ± 0.3 mV.

Table S2. EC_{20} and EC_{50} values of GDN and TBZ for the growth inhibition of *R. subcapitata* and the immobilization of *D. magna*.

Test species	Endpoint	GDN		TBZ	
		EC_{20} (mg/L)			
R. subcapitata	72 h growth inhibition	1.6 ± 0.2		0.24 ± 0.04	
		EC_{50} (mg/L)			
		5.5 ± 0.3		4.5 ± 0.5	
		Without food	With food	Without food	With food
		EC_{20} (mg/L)			
D. magna	24 h Immobilization	16.2 ± 1.7	25.4 ± 2.7	1.8 ± 0.2	2.1 ± 0.2
	48 h Immobilization	5.5 ± 0.3	12.8 ± 0.4	0.65 ± 0.04	0.41 ± 0.05
		EC_{50} (mg/L)			
D. magna	24 h Immobilization	45.1 ± 4.0	73 ± 11	5.3 ± 0.5	5.9 ± 0.6
	48 h Immobilization	7.8 ± 0.3	18.9 ± 0.4	1.3 ± 0.1	0.55 ± 0.02

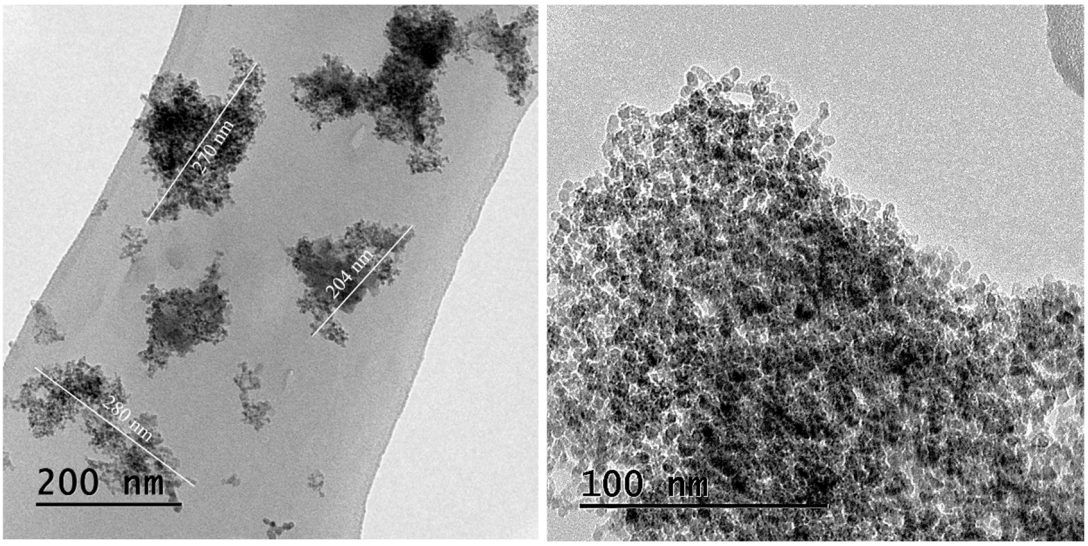

Figure S1. Transmission electro micrographs of GDN suspension in water (10 mg/L) showing the size of aggregates (left) and a detail (right)

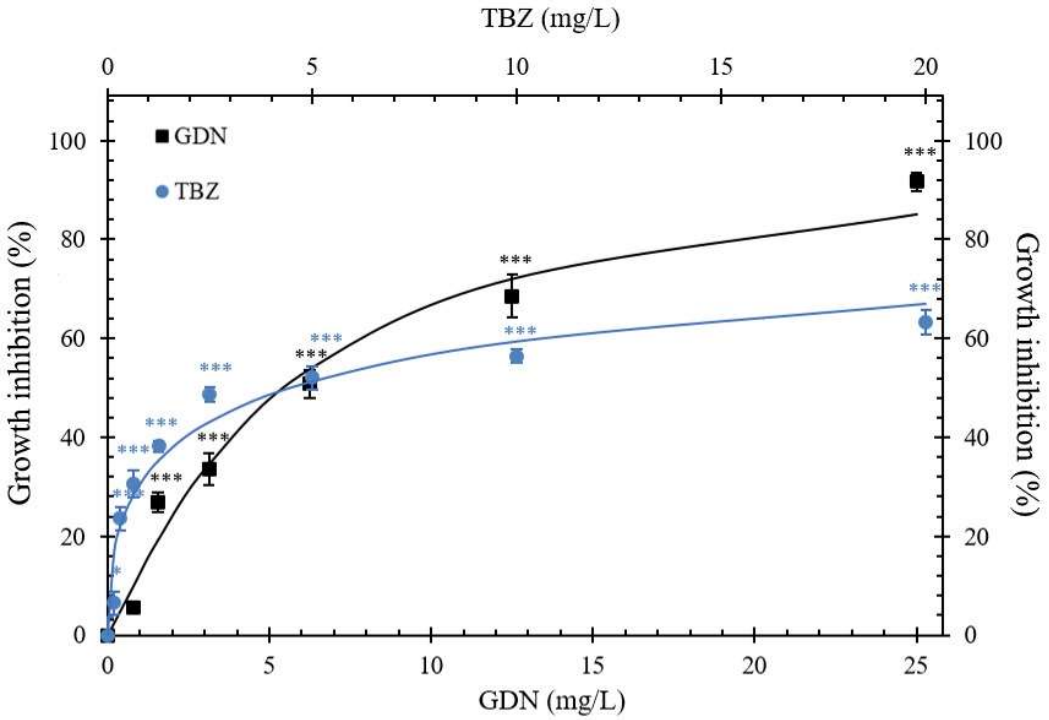

Figure S2. Dose effect response of GDN (♦, lower scale) and TBZ (●, upper scale) for the growth inhibition of *R. subcapitata* (error bars represent standard deviation, n = 6). The lines correspond to the four-parameter log-logistic model used to fit experimental data. Asterisks indicate significant differences from control (Tukey´s HSD, $p < 0.05$).

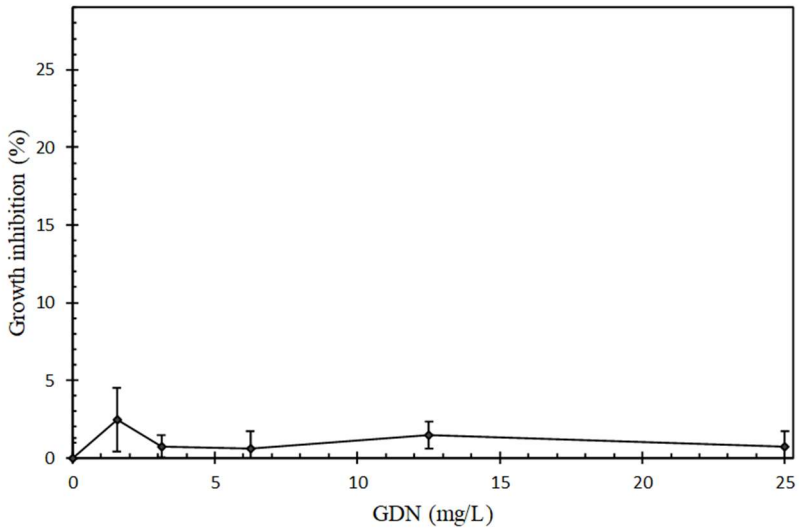

Figure S3. Growth inhibition of *R. subcapitata* due to shading effect of GDN after 72 h.

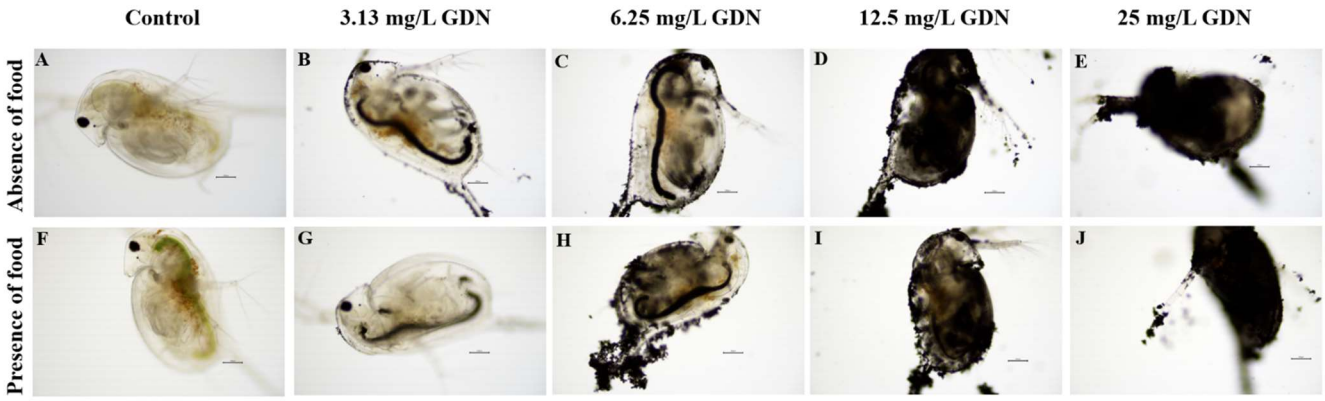

Figure S4. Optical images of *D. magna* after 48 h exposure to 3.13, 6.25, 12.5, and 25 mg/L GDN in the absence and presence of food.

Table S3. Summary of the MIXTOX analysis for *D. magna* exposed for 48 h to GDN-TBZ mixtures in the absence of food (*R. subcapitata*)

	CA					IA			
	Reference	S/A	DR	DL		Reference	S/A	DR	DL
μ_{max}	0.98	0.98	0.98	0.98		0.98	0.98	0.98	0.98
β_{GDN}	5.53	4.90	6.41	4.52		4.50	4.49	4.58	5.91
β_{TBZ}	2.83	3.02	2.98	2.80		2.40	2.40	3.20	3.23
EC_{50GDN}	8.86	9.25	8.61	9.37		7.90	7.90	8.80	9.36
EC_{50TBZ}	0.69	0.79	0.99	0.77		0.52	0.52	0.96	0.89
a	-	-0.67	-4.74	0.01		-	-5.59	-10.10	-6.26
b_{GDN}	-	-	6.93			-	-	9.26	
b_{DL}	-	-	-	46.64		-	-	-	0.22
SS	56.87	55.41	27.69	55.10		76.88	71.73	43.10	52.34
R^2	0.88	0.88	0.94	0.88		0.84	0.85	0.91	0.89
χ^2	409.19	1.46	27.72	0.31		389.18	24.50	9.28	19.39
p	2.9×10^{-87}					6.1×10^{-83}			
$p(\chi^2)$		0.227	1.4×10^{-7}	0.580			0.023	0.002	0.835

Notes: μmax control response (maximum mobility in the absence of both compounds); β slope of the individual dose-response curve for each compound; S/A, DR, DL, a, b_{DL}, and b_{GDN} as defined in Table 1; SS sum of squared residuals; χ^2 test statistic; p is the significance to the CA or IA model fit; $p(\chi^2)$ outcome of the likelihood ratio test where S/A is compared to CA or IA, DR and DL compared to S/A; R^2 maximum likelihood coefficient.

Table S4. Summary of the MIXTOX analysis for *D. magna* exposed (48 h) to GDN-TBZ mixtures in the presence of food. (Notes as in Table S3.)

	CA					IA			
	Reference	S/A	DR	DL		Reference	S/A	DR	DL
μ_{max}	0.98	0.98	0.98	0.98		0.98	0.98	0.98	0.98
β_{GDN}	2.91	2.64	2.61	4.64		2.13	2.37	2.63	4.58
β_{TBZ}	1.46	1.54	1.55	2.37		1.29	1.48	1.51	3.14
EC_{50GDN}	21.56	24.92	25.24	23.36		20.43	24.76	25.91	21.56
EC_{50TBZ}	0.78	0.93	0.92	0.92		0.71	0.91	0.88	0.84
a	-	-1.24	-0.85	-3.57		-	-2.14	-0.95	-7.56
b_{GDN}	-	-	-0.76	-		-	-	-2.97	-
b_{DL}	-	-	-	0.73		-	-	-	1.54
SS	79.12	75.63	75.45	59.97		89.14	82.18	80.57	62.67
R^2	0.72	0.73	0.73	0.79		0.68	0.71	0.71	0.78
χ^2	199.82	3.49	0.17	15.66		189.80	6.96	1.6	19.51
p	4.1×10^{-42}					5.9×10^{-40}			
$p(\chi^2)$		6.2×10^{-2}	0.677	7.6×10^{-5}			8.3×10^{-3}	0.205	10×10^{-6}

Notes: same as Table S3.

Table S5. Dose-effect relationship parameters of GDN, TBZ and GDN-TBZ mixtures.

		Dose-effect parameters		
	Drug/Combo	EC_{50}	m	r
Absence of food	GDN	6.1	3.1	0.85
	TBZ	1.1	2.7	0.93
	GDN+TBZ	1.9	1.8	0.90
Presence of food	GDN	34	2.7	0.82
	TBZ	0.87	3.6	0.87
	GDN+TBZ	7.2	1.4	0.84

The parameters EC_{50}, m and r are the slope, the antilog of x-intercept and the linear correlation coefficient of the median-effect plot, signifying the shape of the dose-effect curve, the potency (EC_{50}), and the conformity of the data to the mass-action law, respectively. $m > 1$ corresponds to sigmoidal dose-response curves; also shown in the table, linear regression correlation coefficients (r-values) of the median-effect plots were > 0.8 in all cases, indicating conformity of the data to the median-effect principle.

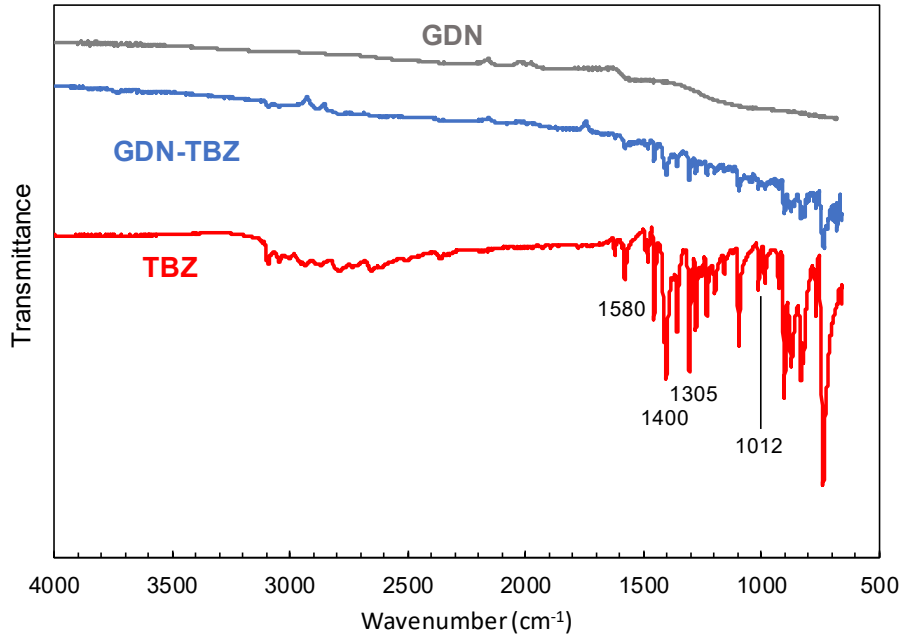

The bands at 1013-982 cm^{-1} corresponded to C-S stretching, the absorption in the 3050-3080 cm^{-1} region corresponded to C-H stretching from aromatic rings, the band at 1550 was due to aromatic ring stretching, and the bands at 1305 and 1280 cm^{-1} correspond to the C-N stretching of tertiary and secondary amines, respectively. The absence of N-H stretching was probably due to the formation of hydrogen bonding, which causes a shift toward lower frequencies and broadens peaks. N-H bending, however, appeared at 1620 cm^{-1}. No significant peaks were observed in the FTIR spectrum of GDN in agreement with their graphitic surface (Ţucureanu V., Matei A. Avram A.M., FTIR spectroscopy for carbon family study, Critical Reviews in Analytical Chemistry, 2016; 46:502-520).

Figure S5. FTIR spectra of GDN, TBZ and GDN after 24 h in contact with TBZ in the same proportions than their respective EC_{50} concentrations (GDN-TBZ).